BUTTERWORTH HEINEMANN

0141-0296(95)00118-2

Engineering Structures, Vol. 17, No. 10, pp. 687–695, 1995

0141-0296/95 $10.00 + 0.00

Combined axial and lateral responses of tensioned buoyant platform tethers

M. H. Patel and H. I. Park*

Santa-Fe Laboratory for Offshore Engineering, Department of Mechanical Engineering, University College London, Torrington Place, London WC1E 7JE, UK

(Received February 1994; revised version accepted March 1995)

This paper presents the results of an investigation into the combined axial and lateral vibrations of the tethers of tensioned buoyant platforms, (TBPs). Wave-induced motions of the TBP excite tether vibrations through lateral forces at the tether top end (called external or forcing excitation in this paper) combined with a time-varying axial force (called parametric excitation here). Although, the forcing and parametric excitations have been considered separately in the research literature, this paper examines their combined effects – particularly with a view to determining tether behaviour for different water depths. The governing partial differential equation of tether lateral motion is reduced to a nonlinear differential equation and solved by a combination of the Romberg method and the fourth-order Runge–Kutta method. Comparisons for tether vibrations when taking both axial and lateral forcing into account and when considering axial and lateral forcing separately are presented. It is shown that the combined excitation gives greater amplitude of vibration with this feature being particularly dominant in even numbers of the instability region of the Mathieu stability chart. The frequency of oscillation of the combined response is also dependent on the relative magnitudes of axial and lateral excitations. The results demonstrate that the above is true for a wide range of water depths.

Keywords: tensioned buoyant platforms, tethers, vibrations

1. Introduction

Tensioned buoyant platforms (TBPs), such as those shown in *Figure 1*, are a class of floating structures that use vertical tethers kept in tension by excess surface platform buoyancy to maintain station in a horizontal plane and to keep heave, roll and pitch responses at very low levels compared to freely floating platforms. The mean tensions are set at relatively high levels to maintain tether tension in combinations of extreme waves, tide levels and platform offset. These high values of mean tension also impose payload, and structural weight penalties. Very many research investigations and much design engineering has been carried out to understand and optimize platform and tether behaviour. A few typical examples of such work are given in References 1–5.

The tethers of TBPs are subjected to two sources of dynamic excitation: the first is motion induced by horizontal platform oscillations which are essentially a forcing excitation whereas the second source of dynamic excitation is due to changes in tether axial force due to variations in vertical force on the platform, called parametric excitation. Much research work has been carried out on each of these excitation sources applied separately to TBP tethers. The horizontal top end forcing excitation problem has been extensively researched, Reference 6 gives a review and Reference 7 presents a typical investigation. The parametric excitation problem – that of determining lateral vibration of the tether induced by time-varying axial force – has been investigated by Hsu[8], and Strickland and Mason[9] among others. Many examples of parametric excitation problems are given in Reference 10 whereas References 11 and 12 examine the problem for drill pipes and for general slender structures, respectively.

* Present address: Department of Ocean Engineering, Korea Maritime University Youngdo-ku, Pusan 606-791, Korea

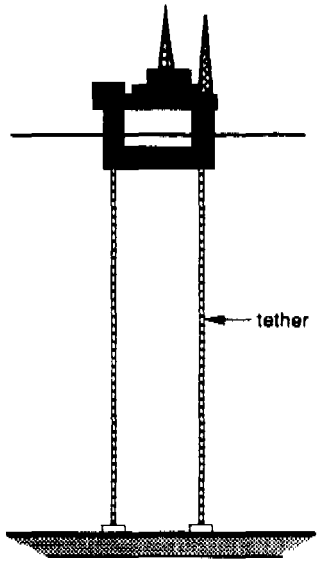

Figure 1 Typical TBP configuration

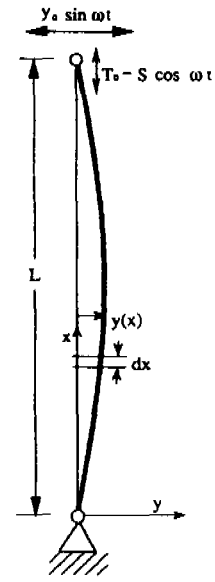

Figure 2 Model structure configuration and notation

This paper presents an analysis for the combined forcing and parametric excitation of TBP tethers. Research work on such combined excitation has only been carried out over the last two decades[13-16]. However, none of these have looked specifically at TBP tethers which are subjected to relatively high tensions compared to other slender structures used in the oceans, such as marine risers. Furthermore, other research in this area has not included nonlinear fluid damping which is a key feature of the problem. These two factors are the principal motivations for the work presented in this paper.

The results of the analysis are illustrated by computing three example cases where tether responses due to combined excitation are compared with computations utilizing forcing or parametric excitation only.

2. Development of theory

A generalized TBP tether is idealized as a straight, simply supported column of uniform cross-section. *Figure 2* shows the idealized configuration under combined excitation and gives the notation being used. The governing equation of lateral motion for the tether is written as

$$M \frac{\partial^2 y}{\partial t^2} + EI \frac{\partial^4 y}{\partial x^4} - (T_0 - S \cos \omega t) \frac{\partial^2 y}{\partial x^2} + B_v \left|\frac{\partial y}{\partial t}\right| \frac{\partial y}{\partial t} = 0 \qquad (1)$$

where M is the total physical plus hydrodynamic added mass per unit length of the tether, EI is the structure flexural rigidity, T_0 is the constant axial tension, S is the time-varying axial force amplitude, ω is the angular frequency of the time-varying axial force (parametric excitation) and $B_v = 0.5\, C_D\, \rho_w\, d_o$, where C_D is a drag coefficient, d_o is the outer diameter of the structure and ρ_w is the sea water density. The tension T_0 is taken to be constant here so as to develop analytic results demonstrating the effects of combined forcing on tethers with tensions that are high compared to their self-weight. Following the same argument, the time-varying axial force is assumed to be sinusoidal. However, the formulation of the equation does include the nonlinear drag-induced damping force. This governing equation excludes the effects of axial elasticity of the tethers on the basis that, for the typical TBP tether lengths considered here, the frequencies of excitation do not excite axial vibration modes. Even in conditions where this does happen, tether axial elasticity can be included reasonably easily in this analysis. However, it has been excluded here for the above reason.

The partial differential equation (1) is reduced to an ordinary nonlinear differential equation by using the method of separation of variables. As can be seen in *Figure 2*, since both ends of the structure are pinjointed, its modes of motion can be readily reduced to a rigid body mode and sinusoidal elastic response modes. Then using the time-dependent boundary condition theory[12] and taking the first four modes for the elastic response mode shapes, an approximate solution to equation (1) is written in the form

$$y(x,t) = h(t) \frac{x}{L} + \sum_{n=1}^{4} f_n(t) \sin \frac{n\pi x}{L} \qquad (2)$$

where L is the length of the structure, $f_n(t)$ is an unknown function of time (a generalized co-ordinate) and $h(t)$ is a prescribed lateral movement of the top end of the structure imparted by surface platform surge motion. This prescribed lateral movement will, of course, modify the time-varying axial force, $-S \cos \omega t$, and its effect has to be incorporated within this force. Only the first four modes are considered so as to simplify the computational effort and at the same time maintain a reasonable level of accuracy. The tether is pinjointed at the top and bottom and for the analysis, the initial position of the top end is set to be at the midpoint of surge motion and in the lowest position of heave motion.

In addition, the top end is taken to rotate in the clockwise direction by the wave-induced surface platform motion. Therefore, $h(t)$ can be written as

$$h(t) = -y_0 \sin \omega t \tag{3}$$

where y_0 is the lateral displacement amplitude and ω is the angular frequency of the top end lateral motion (forcing excitation). Note that since they both stem from a single source, the angular frequencies of parametric excitation and forcing excitation are the same but the phase angle difference between the two excitations is 90°.

Substituting equations (2) and (3) into equation (1) gives

$$\begin{aligned} &M \sum_{n=1}^{4} \frac{d^2 f_n}{dt^2} \sin \frac{n\pi x}{L} + \sum_{n=1}^{4} \left\{ \left[EI \left(\frac{n\pi}{L} \right)^4 \right. \right. \\ &\left. \left. + (T_0 - S \cos \omega t) \left(\frac{n\pi}{L} \right)^2 \right] \sin \frac{n\pi x}{L} \right\} f_n \\ &+ B_v \left| -\frac{x}{L} y_0 \omega \cos \omega t + \sum_{n=1}^{4} \sin \frac{n\pi x}{L} \frac{df_n}{dt} \right| \\ &\cdot \left\{ -\frac{x}{L} y_0 \omega \cos \omega t + \sum_{n=1}^{4} \sin \frac{n\pi x}{L} \frac{df_n}{dt} \right\} \\ &= -\frac{xM}{L} y_0 \omega^2 \sin \omega t \end{aligned} \tag{4}$$

Following Galerkin's method, equation (4) is multiplied throughout by $\sin (m\pi x/L)$ and integrated over the length of the structure, to give

$$\begin{aligned} &\frac{d^2 f_m}{dt^2} + (\bar{\omega}_m^2 - c_1 \cos \omega t) f_m + \frac{2B_v}{ML} \int_o^L \\ &\left| -\frac{\omega y_0 x}{L} \cos \omega t + \sum_{n=1}^{4} \sin \frac{n\pi x}{L} \frac{df_n}{dt} \right| \\ &\left\{ -\frac{\omega y_0 x}{L} \cos \omega t + \sum_{n=1}^{4} \sin \frac{n\pi x}{L} \frac{df_n}{dt} \right\} \sin \frac{n\pi x}{L} dx \\ &= (-1)^m \frac{2y_0 \omega^2}{m\pi} \sin \omega t \end{aligned} \tag{5}$$

where

$$\bar{\omega}_m^2 = \frac{EI}{M} \left(\frac{m\pi}{L} \right)^4 + \frac{T_0}{M} \left(\frac{m\pi}{L} \right)^2 \text{ and } c_1 = \frac{S}{M} \left(\frac{m\pi}{L} \right)^2 \tag{6}$$

$\bar{\omega}_m$ in equation (6) represents the natural frequency of the mth mode of the structure.

It is useful to introduce the nondimensional terms

$$F_m = f_m/d_0, \quad Y_0 = y_0/d_0, \quad X = x/L, \quad \tau = \omega t \tag{7}$$

Then, equation (5) becomes, in nondimensional form

$$\begin{aligned} &\frac{d^2 F_m}{d\tau^2} + (\alpha - \beta \cos \omega t) F_m + c \int_o^1 \\ &\left| -Y_0 X \cos \tau + \sum_{n=1}^{4} \sin n\pi X \frac{dF_n}{d\tau} \right| \cdot \\ &\left\{ -Y_0 X \cos \omega t + \sum_{n=1}^{4} \sin n\pi X \frac{dF_n}{d\tau} \right\} \sin m\pi X \, dX \\ &= (-1)^m \frac{2Y_0}{m\pi} \sin \tau \end{aligned} \tag{8}$$

where

$$\alpha = \left(\frac{\bar{\omega}_m}{\omega} \right)^2, \quad \beta = \frac{S}{EI(m\pi/L)^2 + T_0} \left(\frac{\bar{\omega}_m}{\omega} \right)^2$$
$$c = \frac{2B_v d_0}{M} \tag{9}$$

Equation (8) represents vibrations of a tether subjected to combined parametric and forcing excitation. The lateral response of the tether strongly depends upon β/α and Y_0 which are referred to here as the strengths of parametric excitation and forcing excitation, respectively. The hydrodynamic damping related coefficient, c, plays a role in limiting the response of the combined excitation. If F_m is obtained by solving equation (8), the lateral responses of the structure under combined excitation can be obtained by substituting F_m into equation (7) and then f_m into equation (2). Adequate techniques are not available to give an analytical solution of equation (8), especially for large values of α and β. Therefore, it is necessary to employ a numerical method.

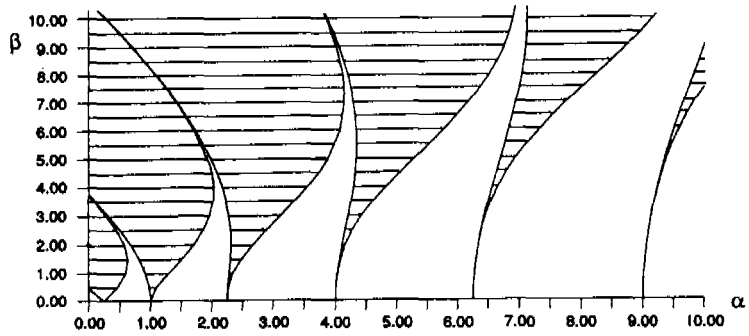

Figure 3 Mathieu stability chart (shaded areas are unstable)

Table 1 Physical data for example structures for case study

Dimension	Case I	Case II	Case III
Length (m)	1520	760	300
Dry mass (kg/m³)	726.3		
Flexural rigidity (N m²)	14.57×10^8		
Inner diameter (m)	0.762		
Outer diameter (m)	0.812	All are the same as case I	All are the same as case I
Added-mass coefficient	1.0		
Hydrodynamic drag coefficient	0.8		
Excitation period (s)	15		
Top tension (N)	13.0×10^6		

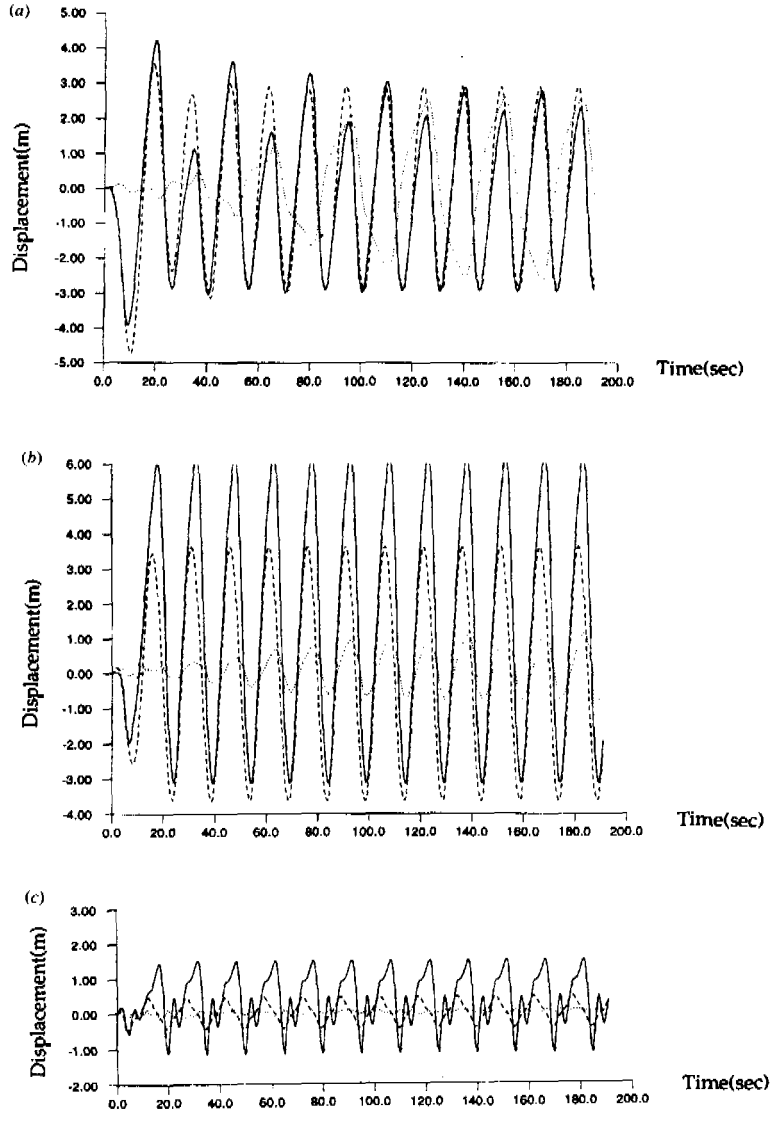

Figure 4 Comparison of lateral displacements of example structures under combined, forcing and parametric excitations for $\beta/\alpha = 1.0$ and $\gamma_0 = 3.0$ m. (a) case I structure (first instability region); (b) case II structure (second instability region); (c) case III structure (fifth instability region). —— combined excitation; --- forcing excitation; ····· parametric excitation

Before carrying out a numerical analysis, it is worth examining equation (8) further. First, if the time-varying axial force, $S \cos \omega t$, is not considered, that is, if $\beta = 0$ in equation (9), the resulting motion of the structure becomes a forced vibration. An analytical solution of forced vibrations can be obtained using an iterative procedure. When the hydrodynamic damping effect is also excluded, the steady-state solution is of the form (see also Reference 18)

$$F_m(\tau) = \frac{(-1)^m 2Y_0}{(\alpha - 1)m\pi} \sin \tau \quad \text{or}$$

$$f_m(t) = \frac{(-1)^m 2y_0 \omega^2}{(\bar{\omega}_m^2 - \omega^2)m\pi} \sin \omega t \tag{10}$$

This result corresponds to the solution of undamped forced vibrations of the tether. However, when the hydrodynamic damping force is considered, the amplitude of the resonance response is limited.

Furthermore, if the lateral motion of the top end is not considered, that is, if Y_0 is zero, equation (8) yields parametrically excited vibrations of the structure which are described by a nonlinear Mathieu equation. An approximate analytical solution of the vibration can be obtained for small values of the parameters, α and β, by using perturbation techniques and can be expressed in the form[8]

$$F_m(\tau) = a_N \cos\left(\frac{N\tau}{2} + \theta_N\right) + (\text{higher order terms}) \tag{11}$$

with the response amplitude, a_N, and the phase angle, θ_N, being function of α, β, m and c. Here N is a positive integer and indicates the number of the instability region along the α axis of the Mathieu stability chart.

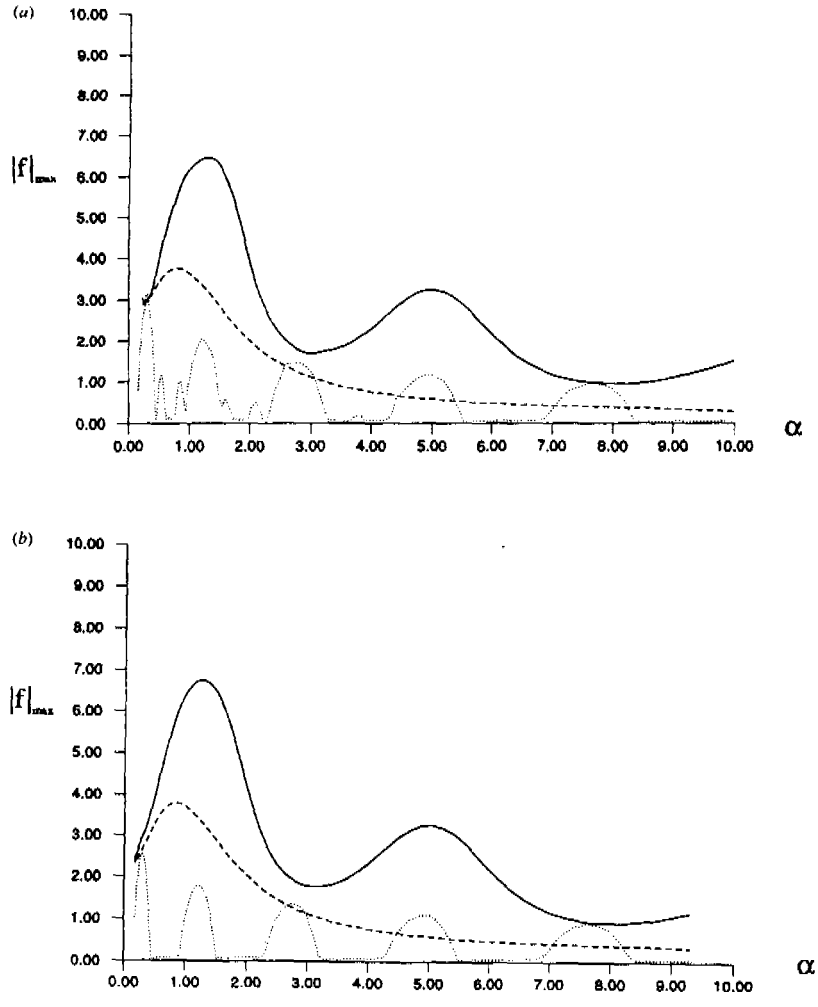

Figure 5 Comparison between frequency response curves of combined, forcing and parametric excitations for $\beta/\alpha = 1.0$ and $y_0 = 3.0$ m. (a) first three modes are considered; (b) only first mode is considered. (Key as in *Figure 4*)

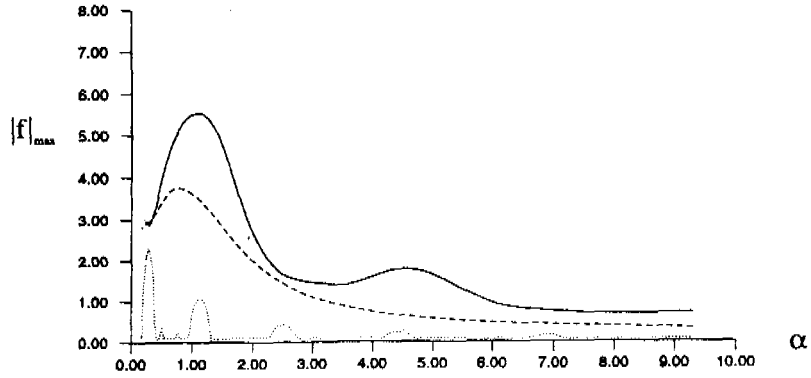

Figure 6 Comparison between frequency response curves of combined, forcing and parametric excitations for $\beta/\alpha = 0.8$ and $y_0 = 3.0$ m. (Key as in *Figure 4*)

However, for larger values of these parameters, a numerical method is necessary. When the hydrodynamic damping force is excluded, the response to the parametric excitation becomes stable or unstable depending on the combination of parameters, α and β, as can be seen from *Figure 3*. However, when the nonlinear hydrodynamic damping force is included, even unstable solutions are limited in amplitude.

3. Results and discussion

Equation (8), which describes a combined excitation problem, is solved using the fourth-order Runge–Kutta method with an extension to take account of the integral term in the equation. This extension is made using the Romberg method to evaluate the integral term at each time step. The source programs for these numerical methods are taken from Reference 19. The initial conditions employed in this study are $F_m(0) = 0.123$ and $dF_m(0)/d\tau = 0.0$, the value for $F_m(0)$ used is typical of that encountered in practice for the tether cases considered here.

Results from the analysis are illustrated using example TBP tethers with the physical data as presented in *Table 1*. Three different tether lengths of 1520, 760 and 300 m are chosen but other parameters such as pretension, structure diameter etc. are taken to be identical to each other for convenience. In the following analysis, 1520, 760 and 300 m lengths will be called case I, II and III structures, respectively, and $c = 0.43$ is used.

The worst sea state is an important environmental condition for the design of TBPs and is thus considered here. In such a condition, 15 s is a typical ocean wave period and is used here as an excitation period. In this worst sea state, the ratio of time-varying axial force amplitude to pretension, S/T_0 ($\cong \beta/\alpha$), has been calculated to be approximately 1.0 for TBP tethers. The amplitude of the top end lateral displacement, y_0, is assumed to be in the range 1.0–5.0 m which corresponds to the ratio amplitude operator (RAO) being 0.07–0.33 for 15.0 m of ocean wave amplitude. In the following analysis, the lateral responses of the structures are obtained at their midpoints.

From *Table 1* and, equations (6) and (9), the values of α_1 for the case I, II and III tethers become 0.25, 1.0 and 6.5, respectively. Therefore, the dominant dynamic condition (or fundamental vibration mode for the case I, II and III tethers corresponds to the first, second and fifth insta-

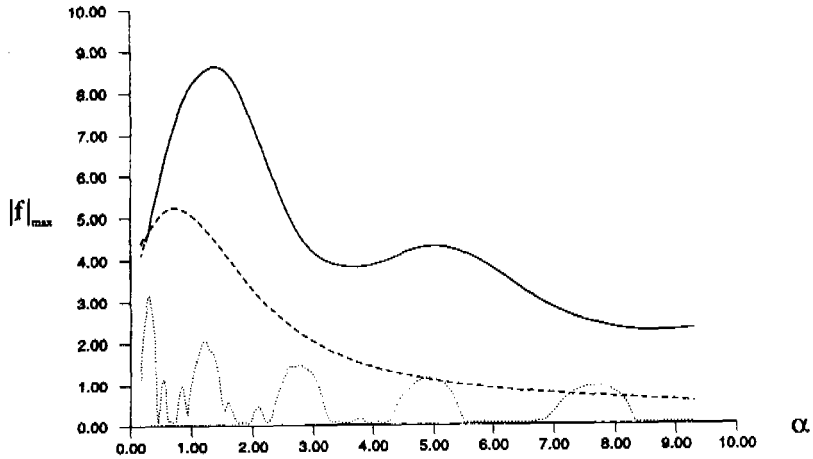

Figure 7 Comparison between frequency response curves of combined, forcing and parametric excitations for $\beta/\alpha = 1.0$ and $y_0 = 5.0$ m. (Key as in *Figure 4*)

bility regions of the Mathieu stability chart (*Figure 3*), respectively.

Although tethers are, in reality, subjected to combined parametric and forcing excitation, the two excitations have been separately considered in most research work. Therefore, comparisons between forcing, parametric and combined excitations are made here to investigate the significance of combined excitation. The comparison is carried out for the lateral displacements of case I, II and III tethers. For the validity of the comparison, the strengths of parametric excitation and forcing excitation, β/α and y_0, are taken to be equal to 1.0 and 3.0 m, respectively, for the three tethers.

Figure 4a shows a comparison between forcing, parametric and combined excitations for the case I (1520 m length) tether. The response amplitudes of the three excitations are nearly identical at the steady state. It can be seen that in this first instability region, there is no recognizable interaction between forcing and parametric excitations to increase the response amplitude of the combined excitation. Meanwhile, the response periods of forcing and parametric excitations are, respectively, identical to and double the 15 s excitation period. This is an expected characteristic of forcing and parametric excitations as can be seen from equations (10) and (11). In the case of combined excitation, the response period is identical to the excitation period. However, if the relative strengths of the excitations, β/α and y_0, change, the response period of the combined excitation can also change as will be shown later.

Figure 4b presents results for the case II (760 m length) tether with a dominant dynamic condition falling in the second instability region. *Figure 4b* shows that the relative response amplitudes of the three excitations in the second instability region are quite different from those in the first instability region (*Figure 4a*). In the second instability region, the response amplitudes of the combined excitation are much larger than those of the forcing or parametric excitation. This means that the interaction between forcing and parametric excitations is significant in the second instability region. The response periods of the three excitations are all the same as for the 15 s excitation period.

Figure 4c illustrates the result for the case III structure with a dominant dynamic condition which corresponds to being in the fifth instability region. The response amplitude

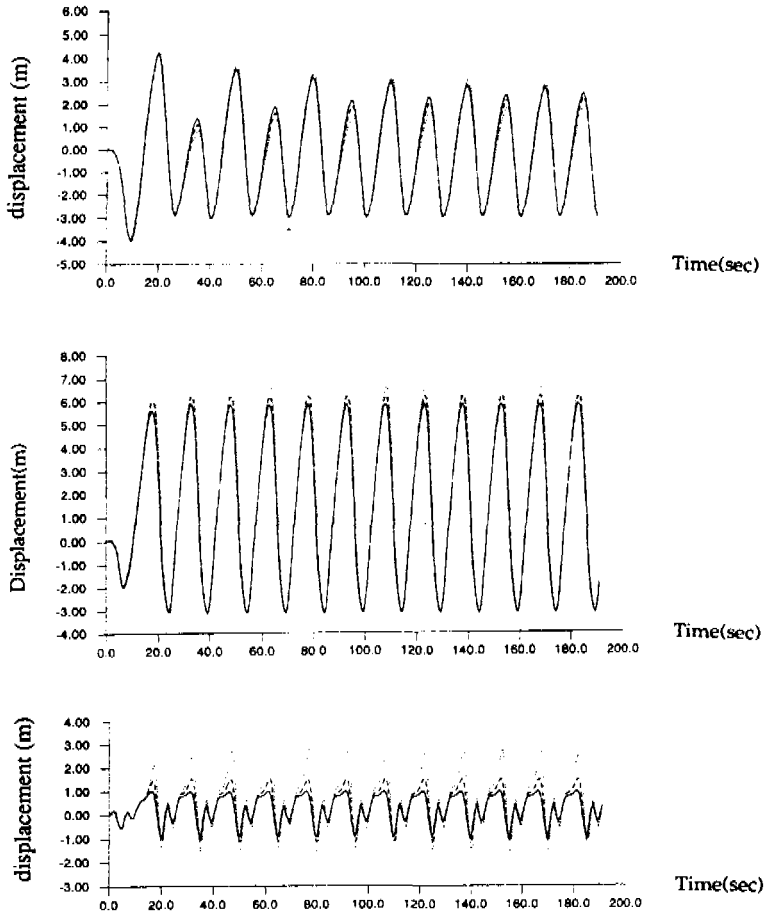

Figure 8 Comparison of lateral displacements of example structures under combined excitation for three different ratios of β/α. Here $y_0 = 3.0$ m is used. (a) case I structure (first instability region); (b) case II structure (second instability region); (c) case III structure (fifth instability region). —— $\alpha/\beta = 0.9$; --- $\alpha/\beta = 1.0$; ····· $\alpha/\beta = 1.1$

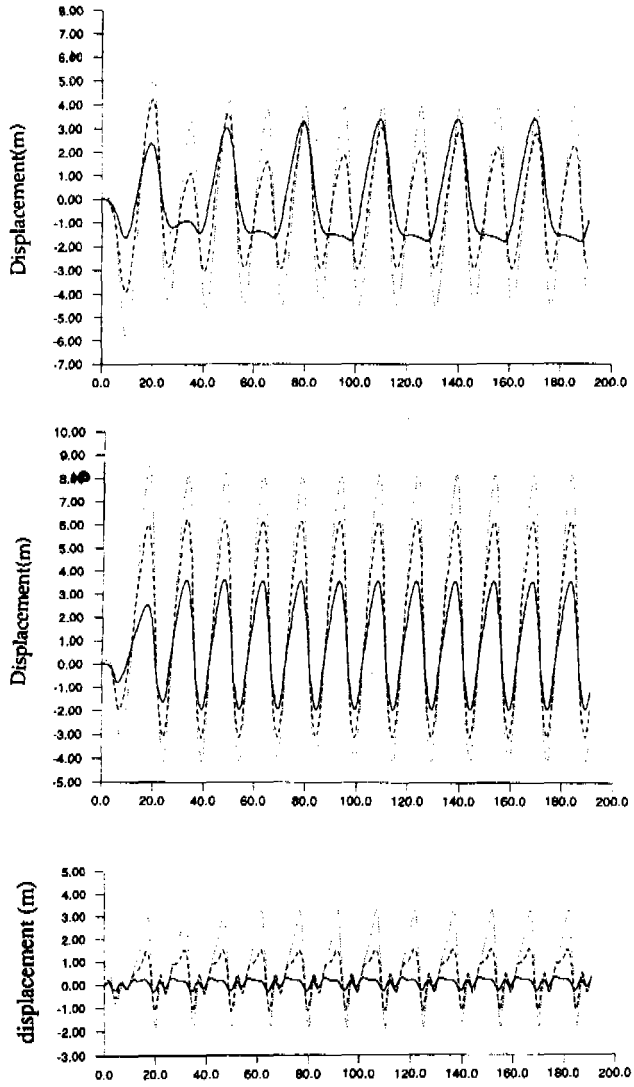

Figure 9 Comparison of lateral displacements of example structures under combined excitation for three different y_0. Here β/α is used. —— $y_0 = 1.0$ m; --- $y_0 = 3.0$ m; ····· $y_0 = 5.0$ m

of the combined excitation is also much larger than that from the forcing or parametric excitation, as for the case II structure. *Figure 4c* indicates that even though the responses of forcing or parametric excitation are small, those of combined excitation are relatively large. The response period of forcing excitation is still the same as the excitation period, 15 s. On the other hand, the response periods of parametric and combined excitations are small compared to the excitation period.

In order to more clearly compare the response amplitudes of forcing, parametric and combined excitations for different instability regions, extensive numerical calculations were carried out. The absolute maximum response amplitude at steady state was obtained for several different tether lengths instead of taking only three lengths as in *Figure 4*. However, the strengths of the excitations, $\beta/\alpha = 1.0$ and $y_0 = 3.0$ m, are kept the same as for *Figure 4*. *Figure 5a* shows the response curves of forcing, parametric and combined excitations as functions of α values. The responses are all limited by the hydrodynamic damping force that is included in the governing equation.

In the case of parametric excitation, large response amplitudes occur in each instability region and their maximum value occurs in the centre of each instability region with the magnitude of the response amplitude decreasing for higher instability regions. The response diagram for combined excitation shows a quite different pattern from those for forcing and parametric excitations with this

response being large in the even numbers of instability regions but relatively small in the odd numbers of instability regions.

In order to test the effect of higher modes of structural vibrations, only the first mode is considered in creating the response curves of the three excitations and the results are shown in *Figure 5b*. By comparing *Figures 5a* and *5b*, it can be seen that the response amplitude with high modes included is only very slightly increased for parametric excitation and vice versa for forcing and combined excitations.

In order to examine the relative dominance of forcing, parametric and combined excitations for different strengths of parametric and forcing excitations, α/β and y_0, the result of *Figure 5a* is investigated further. *Figure 6* shows the effect of decreasing the strength of parametric excitation, β/α ($\cong S/T_0$), from 1.0 to 0.8. The response amplitudes of combined and parametric excitations are both reduced, especially in the high instability regions. There are still considerable differences in the response amplitudes for all three excitations. *Figure 7* presents similar curves with the strength of forcing excitation, y_0, increased from 3.0 to 5.0 m. The response amplitudes of forcing and combined excitations are both increased everywhere compared to *Figure 5a*. The difference of response amplitudes between forcing and combined excitations is substantially increased.

Another aspect of tether response is revealed by presenting time histories of lateral displacements for the three example structures under combined excitation which are obtained for different strengths of parametric and forcing excitations, β/α and y_0. *Figure 8* shows the results for three different strengths of parametric excitation, β/α, with y_0 being kept at 3.0 m for all cases. As the strength of parametric excitation, β/α, increases, the response amplitude of the combined excitation increases for all three structures. However, the increase of response amplitude with strength is more conspicuous in the higher instability regions. The response periods of combined excitation are all the same as the excitation period in the first and second instability regions (*Figures 8a* and *8b*). However, in the case of the fifth instability region (*Figure 8c*), there is a period-doubling phenomenon.

Figure 9 illustrates lateral displacements of the structure under combined excitation for three different strengths of forcing excitation, y_0, with β/α being kept at 1.0 for all cases. As the strengths of forcing excitation increase, the response amplitudes of combined excitation increase in all cases. A particular phenomenon is observed for the case 1 structure (*Figure 9a*) at $y_0 = 1.0$ m, such that its response period is twice the 15 s excitation period. This aspect is different from the cases of $y_0 = 3.0$ and 5.0 m where the response period is the same as the excitation period. It would appear, therefore, that the response period of combined excitation is dependent on the relative strengths of the parametric and forcing excitations.

4. Conclusions

The analysis presented in this paper demonstrates the significant effects of considering the combined forcing and parametric excitation of TBP tethers compared with either of the excitations on their own, as is frequently done in conventional design studies. The analysis has been idealized for computational convenience in that the mean tether tension is taken as constant along its length and only a limited number of tether modes are considered. In particular, the effect of limited tether modes on the computed results is shown to be small.

A general observation from the work is that the response amplitudes from the combined excitations are much larger than those from either parametric or forcing excitations applied separately especially in conditions corresponding to the even numbered instability regions of the Mathieu stability chart. In particular, the largest response amplitudes arise in the second instability region for the assumed mode and the response frequency depends upon the relative strengths of the forcing and parametric oscillation.

References

1 Mercier, J. A. 'Evolution of tension leg platform technology', *Proc 3rd Int. Conf. Behaviour of Offshore Structures*, Massachusetts Institute of Technology, Cambridge, MA, 1982

2 Horton, E. 'Tension leg platform prototype completes Pacific coast test', *Ocean Industry*, 1975, September, pp. 245–247

3 Rainey, R. C. T. 'The dynamics of tethered platforms', Spring Meeting, Royal Institution of Naval Architects, Paper No 6, 1977

4 Faltinsen, O. I., Fylling, I. J., van Hooft, R., Teigin, P. S. 'Theoretical and experimental investigations of tension leg platform behaviour', *BOSS 82*, Vol 1, pp. 411–423, 1982

5 Lyons, G. J. and Patel, M. H. 'Comparisons of theory with model test data for tensioned buoyant platforms', *Trans. ASME, J Energy Res. Technol.* 1984, **106**, 426–436

6 Patel, M. H. and Witz, J. A. 1991, 'Compliant offshore structures', in *Tensioned buoyant platforms*, Butterworth-Heinemann, Oxford 1991, pp. 137–188

7 Jeffery, E. R. and Patel, M. H. 'On the dynamics of taut mooring systems', *J Engng Struct.* 1982, **4**, 37–43

8 Hsu, C. S. 'The response of a parametrically excited hanging string in fluid', *J. Sound Vibr.* 1975, **39**, 305–316

9 Strickland, G. E. and Mason, A. B. 1981, 'Parametric response of TLP tendons – theoretical and numerical analysis', *Proc. Offshore Technol. Conf.* 1981, **3**, 45–54

10 Nayfeh, A. H. and Mook, D. T. *Nonlinear oscillations* John Wiley, New York, 1979

11 Huang, T. and Dareing, D. W. 'Buckling and lateral vibration of drill pipe', *J. Engng for Ind.* 1968, **90**, 613–619

12 Kim, Y. C. and Triantafyllou, M. S. 'The non-linear dynamics of long, slender cylinders', *J. Energy Res. Technol.* 1984, **106**, 250–256

13 Troger, H. and Hsu, C. S. 'Response of a non-linear system under combined parametric and forcing excitation', *J. Appl. Mech.* 1977, **44**, 179–181

14 Thampi, S. K. and Niedzwecki, J. M. 'Parametric and external excitation of marine risers', *J. Engng Mech.* 1992, **118** (5), 942–960

15 HaQuang, N. and Mook, D. T. 'Non-linear structural vibrations under combined parametric and external excitations', *J. Sound Vibr.* 1987, **118**, 291–306

16 Plaut, R. H., Gentry, J. J. and Mook, D. T. 'Non-linear structural vibrations under combined multi-frequency parametric and external excitations', *J. Sound Vibr.* 1990, **140**, 381–390

17 Mindlin, R. D. and Goodman, L. E. 'Beam vibration with time-dependent boundary conditions', *J. Appl. Mech.* 1950, **72**, 377–380

18 Kirk, C. L., Etok, E. U. and Cooper, M. T. 'Dynamic and static analysis of a marine riser', *Appl. Ocean Res.* 1979, **1**, 125–135

19 Press, W. H., Flannery, B. P., Teukolsky, S. A. and Vetterling, W. T. *Numerical recipes – the art of scientific computing* Cambridge University Press, Cambridge, 1989